

Lawrence Berkeley National Laboratory

LBL Publications

Title

Atomic Resolution Observation of the Oxidation of Niobium Oxide Nanowires: Implications for Renewable Energy Applications

Permalink

<https://escholarship.org/uc/item/85w5v3pm>

Journal

ACS Applied Nano Materials, 3(9)

ISSN

2574-0970

Authors

Betzler, Sophia B
Koh, Ai Leen
Lotsch, Bettina V
[et al.](#)

Publication Date

2020-09-25

DOI

10.1021/acsanm.0c01952

Peer reviewed

Atomic Resolution Observation of the Oxidation of Niobium Oxide Nanowires: Implications for Renewable Energy Applications

Sophia B. Betzler,^{*,†,‡,¶,||} Ai Leen Koh,[†] Bettina V. Lotsch,^{‡,¶} Robert Sinclair,[†]
and Christina Scheu[§]

[†]*Materials Science and Engineering, Stanford University, 496 Lomita Mall, CA 94305
Stanford, USA.*

[‡]*Max-Planck Institute for Solid State Research, Heisenbergstraße 1, 70569 Stuttgart,
Germany.*

[¶]*Department of Chemistry, Ludwig-Maximilians-Universität, Butenandtstraße 5-13, 81377
Munich, Germany.*

[§]*Max-Planck Institut für Eisenforschung GmbH, Max-Planck-Straße 1, 40237 Düsseldorf,
Germany.*

^{||}*Sophia B. Betzler, Material Science Department, Lawrence Berkeley National Laboratory,
1 Cyclotron Road, CA 94720 Berkeley, USA.*

E-mail: sbetzler@lbl.gov

Phone: +1 (510) 993 8157

Abstract

Niobium oxide exists in several crystal phases and valence states yielding a variety of properties. Phase transitions between polymorphs significantly alter the properties of functional niobium oxide nanostructures, which are applied in many different renewable energy applications.

This study uses environmental transmission electron microscopy to investigate the oxidation of NbO nanowires to T-Nb₂O₅. Small oxygen partial pressures (< 1 mbar) suffice to initiate the oxidation which initially causes the destruction of the lattice ordering prior to the crystallization of the new phase. Different oxygen partial pressures and temperatures are used to manipulate the reaction kinetics. The crystallization is slow at room temperature and confined to the nanowire surface. Elevated temperatures accelerate the crystallization resulting in the transformation of the complete nanowire. The transformation proceeds via dislocations yielding the woven-like structure of the transformed nanowire. Despite the dramatic changes of the atomic composition of the material, an orientation relationship between the different phases is preserved.

The phase transformation of NbO to T-Nb₂O₅ observed *in situ* complies with *ex situ* phase diagrams. This illustrates the importance of environmental transmission electron microscopy for the investigation of oxidation and reduction reactions of metal oxide nanostructures to identify the impact of shape and intrinsic defects.

Keywords

environmental TEM, solid state oxidation, dislocation-mediated transformation, niobium oxide, crystal defects

1 Introduction

Niobium oxides belong to a complex class of materials.¹ Most phases share a common structure unit: NbO₆ octahedra whose connectivity gives rise to a large variety of stoichiome-

tries² yielding different electronic properties.³⁻⁵ Especially one polymorph – orthorhombic T-Nb₂O₅ – has attracted a lot of attention in recent years due to its anomalously fast energy storage behavior through Li⁺ intercalation.⁶⁻⁸ Its crystal structure consists of sheets of edge- and corner-sharing distorted polyhedra yielding natural tunnels which enable fast ionic transport.^{7,8} Other phases were successfully applied as transparent conductive oxide^{9,10} or photoelectrode in dye-sensitized solar cells.^{11,12}

The common NbO₆ structure unit is at the heart of a complex phase space in niobium oxide, making them a great model system for studying phase transformations *in situ*. Central questions about solid-solid transitions focus on their kinetic pathways and the impact of defects formed during the transformation. Hence, dynamic insights into the reactions happening at the atomic scale during solid-solid transitions, which can be provided by *in situ* transmission electron microscopy, are crucial for our understanding of the underlying mechanisms.^{13,14} Solid-solid transitions are induced by a multitude of factors, e.g. temperature, pressure, strain or changes of the atomic composition. Besides classical physical forces, irradiation by high-energy electrons can likewise cause structural transformation in materials due to local heating of the sample,^{15,16} or by changes of the elemental composition due to radiolysis or knock-on damage.¹⁷⁻¹⁹ In this regard, the electron beam induced reduction of Nb₃O₇(OH) to NbO was analyzed in detail using *in situ* TEM experiments.²⁰ A highly intense electron beam and elevated temperatures are required for efficient sputtering of oxygen from the crystal lattice. Initially, the loss of oxygen is compensated by changes of the connectivity of the NbO₆ octahedra. Subsequently, the crystal ordering is lost before NbO crystallizes leading to the formation of pores inside the nanowire to compensate the volume difference between Nb₃O₇(OH) and NbO.²⁰

Environmental transmission electron microscopes (ETEM) enable the investigation of specimen in different gas atmospheres and can be used to study redox reactions, growth phenomena or gas storage with atomic resolution.²¹⁻²⁵ This study uses ETEM to observe the re-oxidation of porous NbO, which was obtained by reducing Nb₃O₇(OH) with the electron

beam following the protocols of previous studies.²⁰ Small oxygen partial pressures (< 1 mbar) suffice to drive the re-oxidation reaction allowing high spatial resolution during the experiment; higher gas pressures in the column enhance scattering of the electron beam reducing the spatial resolution. High resolution images yield new insights into changes of the crystal lattice during the re-oxidation reaction. Different experimental conditions, with respect to sample temperature and oxygen partial pressure, were applied to manipulate the kinetics of the re-oxidation reaction. The experiments yield new insights into the role of dislocations during the phase transformation and their impact on the final crystal structure.

2 Results and discussion

Hydrothermally grown $\text{Nb}_3\text{O}_7(\text{OH})$ nanowires^{26,27} can readily be reduced to NbO by the electron beam if the specimen temperature is above 500 °C. The volume difference between the two phases is compensated by a porous structure formed inside the nanowires as described in detail in previous studies.²⁰ This study focuses on an understanding of the re-oxidation of these porous NbO nanowires induced by the introduction of oxygen into the column of an ETEM (see scheme in fig. 1).

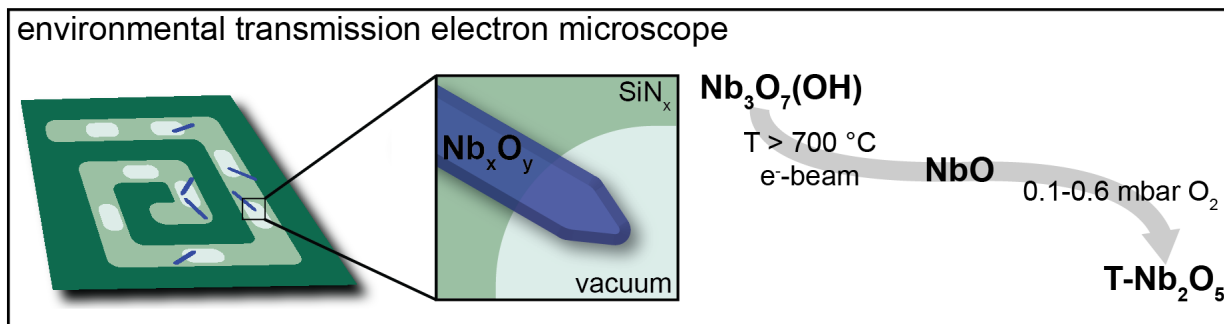


Figure 1: Schematic representation of the reaction performed in this study. A silicon nitride heating chip was used to control the specimen temperature. In a first step the $\text{Nb}_3\text{O}_7(\text{OH})$ nanowires were reduced to NbO by the electron beam, in a second step they were re-oxidized by O_2 introduced into the column of the ETEM.

In situ TEM experiments are sensitive towards artifacts introduced by the electron irradiation. Radiolysis is the dominant damage mechanism in many transition metal oxides.^{28,29}

We therefore used an acceleration voltage of 300 kV to reduce the damage cross-section in our experiments.³⁰ In addition, a recent study demonstrates that a gas atmosphere prevents the electron beam induced reduction of niobium oxides.³¹ The combination of a high acceleration voltage with the presence of a gas atmosphere reduces the impact of the electron irradiation and we therefore assume that electron beam induced changes play a subordinate role in this study. The oxygen partial pressure is increased steadily during the ETEM experiment (from 0 mbar to 0.6 mbar) while monitoring changes of the sample either with electron energy-loss spectroscopy (EELS) or in image mode. The EEL spectra were collected in diffraction mode averaging over a large area of the nanowire concealing local variations of the oxidation state. A quantitative analysis of the O-to-Nb ratio was hindered by the dynamic changes of the oxygen partial pressure during the re-oxidation. Therefore, the valence state of niobium was used as fingerprint by analyzing the electron energy-loss near-edge fine structure (ELNES) of the Nb-M_{2,3} edge: The energy position of the peak maximum of the Nb-M₃ edge was analyzed as a function of the oxygen partial pressure yielding a rapid shift of 0.8 eV from 364.5 eV to 365.3 eV induced by the introduction of less than 0.1 mbar oxygen at room temperature (fig. 2a). The final position of the Nb-M₃ edge was 365.5 ± 0.1 eV for oxygen partial pressures exceeding 0.2 mbar, which agrees well with the energy position of pentavalent niobium (tab. S1).³² This is confirmed by the fine structure of the Nb-M₃ edge, which exhibits a characteristic high energy shoulder for the pentavalent state (fig. 2b). This shoulder is already clearly visible at an oxygen partial pressure of 0.1 mbar, suggesting that the oxidation reaction happens rapidly after oxygen supply. Similarly, the fine structure of the O-K edge shows distinct changes: features I and II have a similar intensity for NbO while the intensity of feature II decreases relative to feature I for pentavalent niobium (fig. 2c). The porous structure of the NbO nanowires most likely assists the oxygen diffusion through the lattice. In this regard, studies demonstrate that interconnected networks of mesopores yield higher diffusion rates,³³ but even isolated mesopores improve diffusivity of guest molecules at elevated temperatures.³⁴

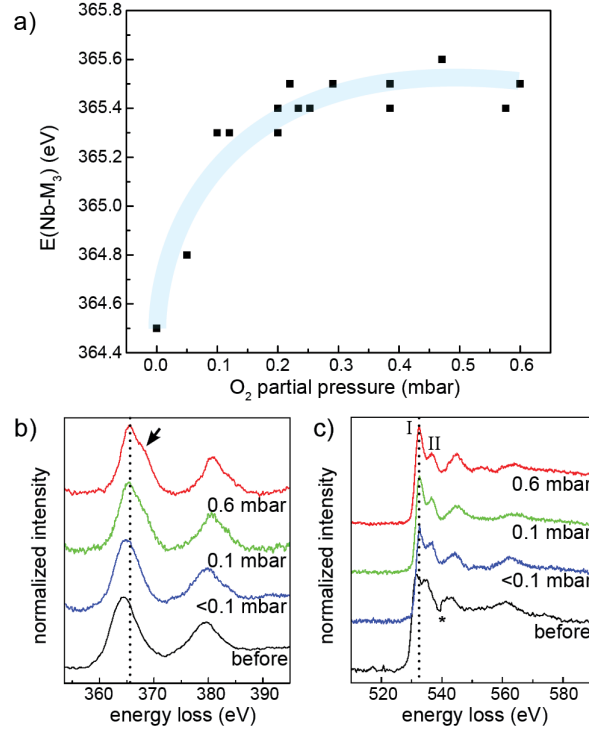


Figure 2: EEL spectra recorded during the re-oxidation of niobium oxide nanowire induced by the introduction of oxygen gas into the TEM column at room temperature. a) Energy shift of the Nb-M₃ edge as a function of the oxygen partial pressure. The oxygen pressure was increased slowly during the experiment: for pressures below 0.21 mbar with a rate of 0.006 mbar/min, for partial pressures above 0.21 mbar with a rate of 0.016 mbar/min, giving the system enough time to equilibrate (see fig. S1). The fine structure of the Nb-M_{2,3} edge (b) and O-K edge (c) observed at specific oxygen partial pressures during the re-oxidation. × * Marks an artifact during spectrum acquisition.

Figure 3a shows TEM images recorded during the re-oxidation of the nanowire at room temperature while gradually increasing the oxygen partial pressure. The re-oxidation of the material causes dramatic changes of the crystal lattice of the nanowire leading to changes of the pore structure depending on the oxygen partial pressure. Hence, we define the *projected pore area*, which describes the area of the pores inside the nanowire relative to the total area of the nanowire, as a quantitative measure for changes of the pore structure. The introduction of small oxygen amounts has a drastic effect on the pore structure of the nanowires. The pores close to the surface disappear featuring a decrease of about 20% projected pore area (fig. 3b). Concurrently, the initially rectangular pores, which are characteristic for *in situ*

reduced NbO, lose their shape and become round. The analysis of the projected pore area indicates a slower filling of the pores subsequent to the filling of the pores close to the surface. This might be related to the limitation of the method which analyzes the two dimensional projection of the pore volume and pore distribution. This can create an error at high pore concentrations due to the overlap of multiple pores in z-direction potentially concealing changes of the pore concentration. However, the analysis of changes of the projected pore area as a function of the oxygen partial pressure indicates slightly faster reaction kinetics for higher oxygen partial pressures (see fig. S2). During our experiments we decided to actively manipulate the reaction speed to reduce the experiment time and steadily enhance the oxygen partial pressure. It is important to note that the nanowire contours coincide before and after the re-oxidation (fig. S3), except for a small deformation of the nanowire tip. This indicates the filling of the pores instead of a shrinking of the nanowire through a redistribution of material during the re-oxidation reaction. Altogether, our experiment shows that the filling of bulk pores is significantly slower than the filling of surface pores. It would be interesting to probe the incorporation process of oxygen at the pore surfaces with localized EELS experiments. Unfortunately, the overlap of multiple pores in z-direction yields a convoluted signal which prevents meaningful results.

The re-oxidation is associated both with an increase in mass and changes of the crystal structure. Fast Fourier transformation (FFT) pattern illustrate the changes of the crystal lattice during the reaction. They show the immediate loss of lattice ordering induced by small oxygen concentrations and only two reflections with a lattice spacing of 2.1 Å (NbO (200)) remain. Subsequently, a new crystal phase, which is characterized by d-spacings of 3.9 Å and 3.2 Å, forms. Bragg filtering identifies the regions of the nanowire which contribute to distinct reflections in the pattern. The analysis demonstrates small NbO islands within the nanowire while small seeds of the new phase form in regions close to the nanowire surface (fig. 4). The size of these crystal seeds increases with time, but even after all pores were filled the crystallization of the new phase is limited to regions close to the nanowire surface. It was

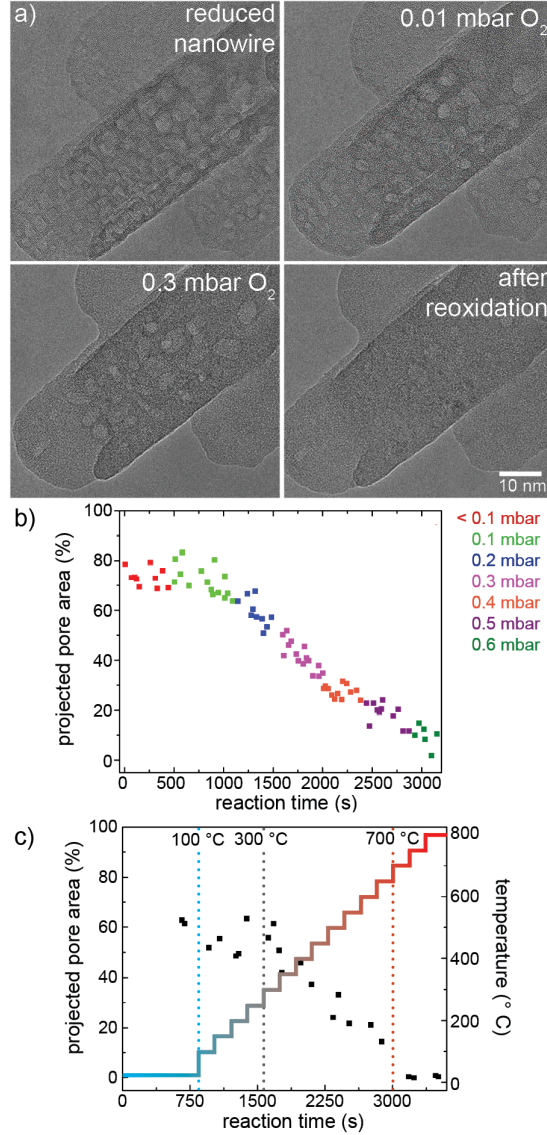


Figure 3: Re-oxidation of NbO nanowires induced by the introduction of oxygen gas. a) TEM images recorded for one nanowire at different oxygen partial pressures at room temperature. The changes of the pore concentration are clearly visible. b,c) Quantitative analysis of the projected pore area, which describes the area of the pores relative to the area of the total nanowire. The data are represented in dependence of the projected pore area before the re-oxidation experiment. b) Projected pore area as a function of the oxygen partial pressure at room temperature (dose rate $3900 \text{ e}^- \text{ \AA}^{-2} \text{ s}^{-1}$). c) Changes of the projected pore area at a constant oxygen partial pressure (0.2-0.3 mbar) but with increasing temperature (dose rate $3100 \text{ e}^- \text{ \AA}^{-2} \text{ s}^{-1}$). The heating profile is superimposed.

not possible to observe the transformation of the complete nanowire within the timeframe of our *in situ* experiments, which can be up to 12 hours.

The crystallization of the new crystal phase is very slow at room temperature which is

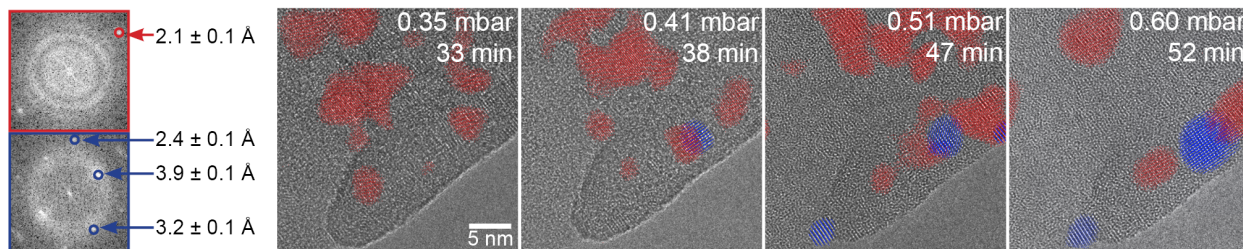


Figure 4: HRTEM images recorded during the re-oxidation of NbO at room temperature (dose rate $3900 \text{ e}^- \text{ \AA}^{-2} \text{ s}^{-1}$). The images show the crystal lattice at different oxygen partial pressures starting with a partial pressure of 0.35 mbar. The analysis focuses on a region at the nanowire surface whose pores were filled due to the exposure to oxygen. Bragg filtering was applied to identify the localization of the two phases (red and blue) in the nanowire at different oxygen partial pressures and reaction times. The respective reference FFT pattern for the two phases are given on the left.

why the re-oxidation experiment was repeated at elevated temperatures: A constant oxygen partial pressure of 0.2-0.3 mbar was used while gradually increasing the temperature to 800 °C. In accordance with the previous experiment the pore density decreases due to the introduction of oxygen, which reflects in a reduction of the *projected pore area* by 40%. In agreement with the experiment at room temperature the projected pore area does not change dramatically up to 300 °C. Higher temperatures increase the reaction kinetics yielding the complete disappearance of the pores within 20 minutes (fig. 3c). Again, most of the lattice ordering is lost due to the introduction of oxygen yielding small NbO islands embedded in an amorphous matrix. Bragg filtering of HRTEM images demonstrates that these crystalline regions decrease in size with increasing temperature and reaction time (see fig. S4 & S5). At 500 °C small crystallites of a new crystal phase appear inside the nanowire (fig. 5). In contrast to the re-oxidation at room temperature, the formation of the new phase is not limited to the surface of the nanowire. We believe that the elevated temperatures and local variations of the elemental composition resulting from the pristine pore structure facilitate the crystallization of the new phase in distinct regions. The number and sizes of its crystallites increase with temperature and time until they cover a significant part of the nanowire at 700-750 °C reflecting in diffusive reflections centered at 3.6 Å in the FFT pattern. The crystallites continue to grow in size while the specimen is kept at 800 °C

ultimately leading to the formation of a woven-like structure. In addition, crystallites with a lattice spacing of 5.0 Å occur (tab. S2). After prolonged calcination times single crystalline regions with lattice spacings of 3.9 Å and 3.2 Å form (fig. S7). These values match the lattice spacings observed for the small crystal grains which form at room temperature (fig. 4).

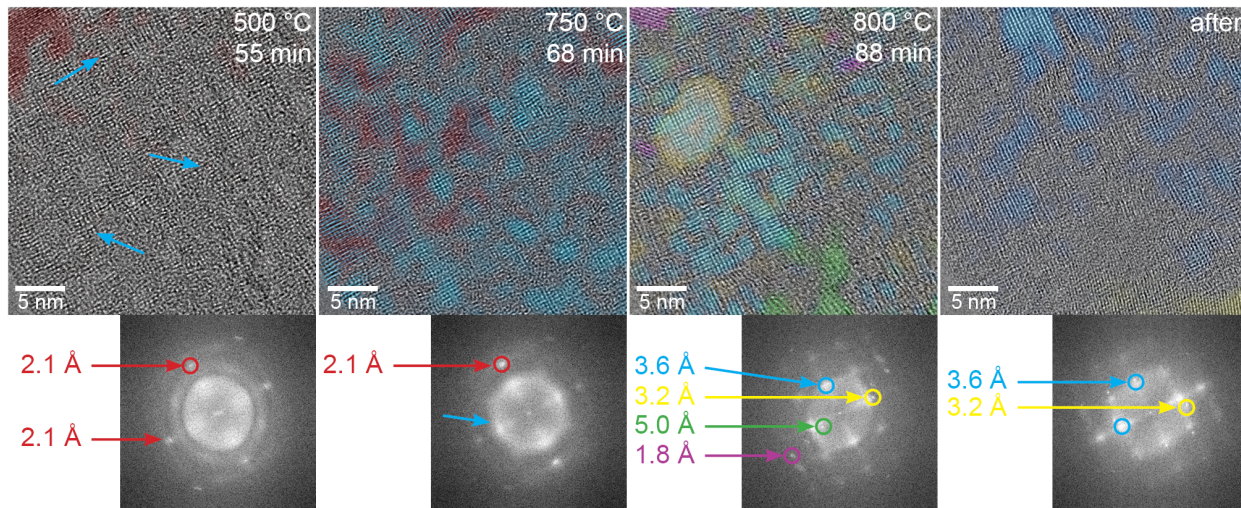


Figure 5: HRTEM images recorded during the re-oxidation performed at constant oxygen partial pressures between 0.2 and 0.3 mbar while gradually increasing the temperature (dose rate $3100 \text{ e}^- \text{Å}^{-2} \text{s}^{-1}$). The heating profile used for the experiment is displayed in fig. S6. The formation of a new phase can first be observed at 500 °C as small crystallites with a larger lattice spacing become visible within the nanowire. Other than observed at room temperature the formation of the new phase is not limited to the nanowire surface. The new phase is more pronounced at 700-750 °C reflecting in diffusive reflections centered at 3.6 Å in the FFT pattern. Calcination at 800 °C yields sharper reflections in the FFT pattern, with lattice spacings of 5.0 Å and 3.2 Å. These reflections result from different crystal orientations of the new phase (see tab. S2). The initial crystals grow in size with continuous heating forming a woven-like pattern.

Rapid re-oxidation – achieved by introducing less than 0.1 mbar O_2 at 850 °C – gives further insights into the mechanism of the re-oxidation reaction (fig. 6). The exposure to oxygen causes dramatic changes of the crystal lattice and the immediate filling of the pores. Lattice planes with a spacing of 3.7 Å form along one direction directly after the exposure to oxygen gas. A high concentration of dislocations is visible within the lattice planes, highlighted in white in figure 6a. The dislocations seem to accumulate in distinct planes, promoting the lattice ordering in the perpendicular crystal direction which ultimately result

in the formation of the woven-like pattern within the crystal lattice. A similar structure was observed during the slow re-oxidation (fig. 5). The concentration of these dislocations decreases with continued heating, however even after 25 minutes at 850 °C a significant number of dislocations remains (fig. S8).

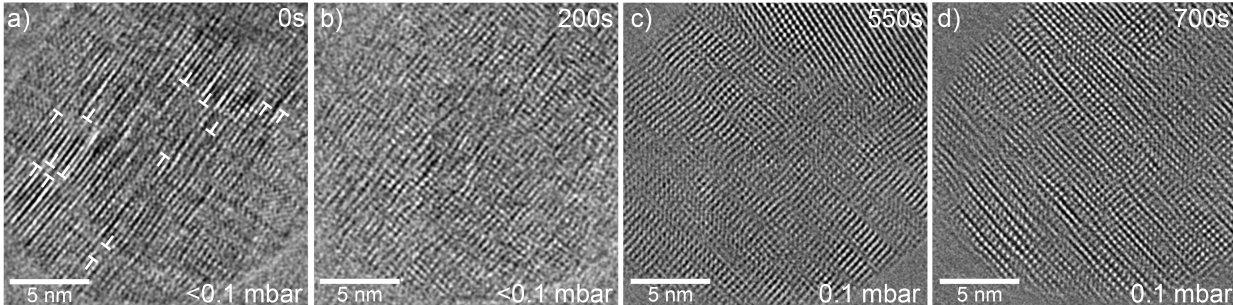


Figure 6: HRTEM images acquired during the rapid re-oxidation of NbO due to the introduction of oxygen at 850 °C (dose rate $1700 \text{ e}^{-}\text{\AA}^{-2}\text{s}^{-1}$). the oxygen partial pressures are indicated in the images. The time was arbitrarily set to the starting time of the imaging. a) Initially crystal lattice planes with a spacing of 3.7 Å form. The lattice contains a high concentration of dislocations which seem to accumulate in distinct planes, exemplary dislocations are highlighted in white. b)-d) the dislocations subsequently promote the establishment of lattice ordering in the perpendicular direction of the crystal lattice. While a high defect concentration is still visible in b) the lattice ordering improves with continuous heating.

The interaction of the electron beam with the oxygen gas alters its reactivity.²² Thus, the re-oxidation experiment was also performed in the absence of the electron beam to avoid the beam effects. High resolution images and electron diffraction experiments yield important insights into the crystal structure of the re-oxidized nanowire (fig. S9). EELS investigations confirm that it was fully re-oxidized to pentavalent niobium oxide (see tab. S1). The niobium oxide system is characterized by a high variety of crystal phases, which complicates the identification of the phases formed during the re-oxidation.^{2,35} The diffraction pattern exhibits a hexagonal symmetry composed of reflections with d-spacings of $3.2 \pm 0.1 \text{ \AA}$ and additional diffuse reflections. Its symmetry suggests a hexagonal crystal structure. TT-Nb₂O₅ is the only niobium phase with a pseudo-hexagonal symmetry (space group P6/mmm)^{36,37} and the observed d-spacing matches its (10 $\bar{1}$ 0) and (1 $\bar{1}$ 00) planes (see table S2). The crystal

structure of TT-Nb₂O₅ is not well understood and is usually described as less-crystalline variation of orthorhombic T-Nb₂O₅. The unit cell of T-Nb₂O₅ comprises 16.8 niobium atoms and is characterized by paired positions close to z=0.5 each with an occupancy factor of 0.5. The additional 0.8 niobium atoms are distributed over sites located in the a-b plane at z=0 with occupancy factors between 0.08 and 0.04 (fig. 7c).³⁸ The structure of TT-Nb₂O₅ can be derived from this structure by assuming that the niobium atoms are not distributed between the two paired sites but instead are located at z=0.5 with an occupancy factor of 1. Unfortunately, this approach solely yields the positions of the niobium atoms relative to the T-Nb₂O₅ unit cell and the exact positions of the oxygen atoms remain unknown.³⁹ The close similarity between and TT-Nb₂O₅ complicates the distinction of the two phases and simulated electron diffraction patterns were used for a better understanding of the experimental pattern. The simulation of T-Nb₂O₅ yields sharp reflections that correlate with the main reflections in the pattern. In addition, it reveals closely spaced reflections that could explain the diffuse reflections observed in the experimental data (fig. S10). The diffraction patterns were simulated for different crystal structures to distinguish T-Nb₂O₅ and TT-Nb₂O₅. The simulations show that the low occupancy niobium positions in the a-b plane cause a pair of two reflections with similar intensities and additional strong reflections close to the primary beam. Hence, the diffuse reflections are reproduced more clearly for T-Nb₂O₅, making it more probable that T-Nb₂O₅ is formed rather than TT-Nb₂O₅. These results match other studies which analyze the crystallization of amorphous Nb₂O₅ respectively NbO₂ during continuous heating in ambient atmosphere.^{36,40} For the sake of simplicity we will limit the following discussion to T-Nb₂O₅, but we cannot rule out the presence of TT-Nb₂O₅ based on the available data. Quantification of EELS data recorded for samples oxidized at 800 °C in the presence and absence of the electron beam yields an atomic O-to-Nb-ratio of 2.5 for both samples (see fig. S11), and no impact of the electron beam on the atomic composition can be detected within the sensitivity of the method. In addition, a previous study shows that an oxygen or nitrogen gas atmosphere can fully pre-

vent the electron beam induced reduction of niobium oxide even at high temperatures and dose rates.³¹ Hence, we assume that the pressure and temperature conditions outweigh the effect of the electron beam during our experiments and predict the formation of T-Nb₂O₅ for all *in situ* re-oxidation experiments performed in this study. In agreement with this assumption we assign the crystals observed during the re-oxidation in the presence of the beam to T-Nb₂O₅ in [010] direction. All d-spacings observed during the oxidation reaction can be assigned to T-Nb₂O₅ (see tab. S2), which suggests that no meta-stable phases occur intermediately during the phase transformation.

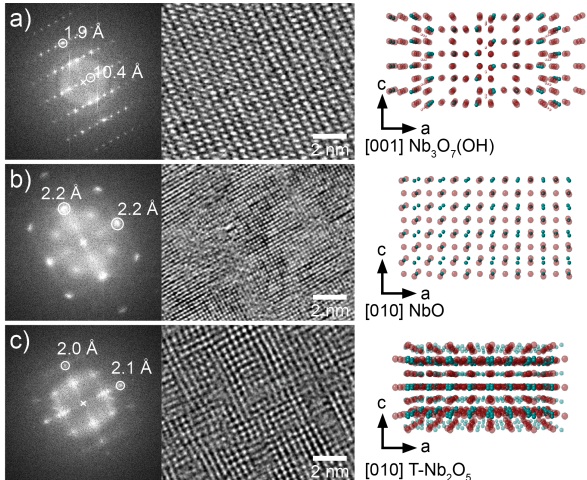


Figure 7: HRTEM images of the crystal structures of the pristine Nb₃O₇(OH) (a), the *in situ* reduced NbO (b) and the re-oxidized nanowire (c). The reoxidation experiment was performed at 850 °C in the presence of 0.2-0.3 mbar oxygen partial pressure. The corresponding FFT pattern and simulations of the crystal structure are displayed in addition.

The data presented here allow the formulation of a mechanistic model for the re-oxidation reaction. Upon exposure to oxygen gas, oxygen diffuses through the NbO crystal lattice. Solid state diffusion of anions/cations in metal oxides often proceeds in the respective sublattice. In this regard, the crystal structure of the material determines the likelihood of either cation or anion diffusion. Cation diffusion is preferred in close packed structures due to the higher formation enthalpies of defects in the anion sublattice. On the contrary, oxygen diffusion dominates in metal oxides with a more open anion sublattice like perovskites or fluorite structures.⁴¹ NbO crystallizes in a defective cubic rocksalt-type structure with the

shortest O-O distance being 2.98 Å (fig. 7b),¹ which is similar to the perovskite structure (2.80 Å).⁴² The open anion sublattice facilitates the diffusion of the oxygen atoms through the anion sublattice via interstitial sites (fig. S12). EELS analysis indicates that low oxygen partial pressures suffice to re-oxidize the material, indicating fast diffusion of oxygen through the crystal lattice even at room temperature. The loss of valence electrons causes a reduction of the ionic radius of the niobium cations.⁴³ These massive changes in both the anion as well as the cation sublattice result in the loss of the overall lattice ordering yielding a predominantly amorphous structure. Initially the porous structure is preserved in the center of the nanowires, but it becomes less pronounced with time and finally disappears indicating the diffusion of both oxygen and niobium atoms. At room temperature the crystallization of the new crystal phase is limited to the nanowire surface, while elevated temperatures help to overcome the activation barrier for the crystallization resulting in the transformation of the complete nanowire. Still, a high defect concentration remains yielding a woven-like structure of the crystal lattice. Interestingly, we find that main crystal directions of the different phases are aligned (fig. 7 and fig. S13), despite the dramatic changes of the atomic composition of the different phases (starting phase Nb₃O₇(OH), reduced phase NbO and re-oxidized phase T-Nb₂O₅). This suggests that the cation sublattice is partly preserved throughout the phase transitions. Considering the Nb-Nb distance (4.2 Å) in the NbO crystal lattice, the pre-ordering explains the initial formation of lattice planes with a spacing of 3.7 Å (fig. 6). The transformation subsequently proceeds via the introduction of dislocations which accumulate in distinct planes. Solid state transformations frequently commence via dislocations, which act as diffusion pathways, release strain and compensate lattice mismatch between phases.⁴⁴⁻⁴⁷ The dislocations mediate the crystallization of T-Nb₂O₅, observed in this study, yielding a woven-like pattern. Continuous heating reduces the defect concentration resulting in small single crystalline regions of T-Nb₂O₅.

3 Conclusion

This study investigates the oxidation of porous NbO nanowires using environmental transmission electron microscopy. We use different oxygen partial pressures and temperatures to manipulate the reaction kinetics to obtain an understanding of the underlying reaction mechanism. The porous morphology and open crystal lattice facilitate the diffusion of oxygen into the nanowires and small partial pressures suffice to completely transform NbO to Nb₂O₅. The diffusion of oxygen through the crystal lattice initially destroys the lattice ordering, before a new phase forms. At room temperature the formation of the new crystal phase is confined to the surface of the nanowire, while higher temperatures accelerate the crystallization reaction so that the complete nanowire transforms. The crystallization of the new phase proceeds via dislocations which initially accumulate in distinct planes and finally yield a complex lattice structure, which resembles a wave-like pattern. Diffraction data indicate that the new phase is T-Nb₂O₅ independent of the conditions used for the re-oxidation. This agrees with the *ex situ* phase diagram of niobium oxide. Despite the drastic changes of the elemental composition an orientation relationship is preserved between the different crystal phases. Most niobium oxide phases consist of NbO₆ polyhedra which might facilitate topochemical phase transitions between different phases. Different niobium oxide phases have profoundly different properties, thus an indepth understanding of the transformation between different phases is critical for their application.

This study illustrates the impact of defect structures on solid-state oxidation reactions. The observed phase transformation complies with the phase diagram of niobium oxide, which illustrates the importance of ETEM for the study of redox reactions of metal oxide nanostructures.

Acknowledgement

This work was performed at the Stanford Nano Shared Facilities (SNSF), supported by the National Science Foundation under award ECCS-1542152. The authors thank goes to Ann F. Marshall and Yuzhang Li for their support with the microscope. S.B.B. furthermore acknowledges financial support provided by the Bavaria California Technology Center (BaCaTeC). S.B.B. and R.S. acknowledge financial support by the Toyota Research Institute, C.S. acknowledges financial support from the German Research Foundation via the grant SCE 634/20-1.

Supporting Information Available

Experimental procedures and additional characterization data can be found in the supporting information.

References

- (1) Brauer, G. Die Oxyde des Niobs. *Zeitschrift für anorganische und allgemeine Chemie* **1941**, *248*, 1–31.
- (2) Nico, C.; Monteiro, T.; Graça, M. Niobium oxides and niobates physical properties: Review and prospects. *Prog. Mater. Sci.* **2016**, *80*, 1 – 37.
- (3) Rüscher, C. The structural effect on the electrical properties of $\text{NbO}_{2.5-x}$ block-type compounds. *Physica C* **1992**, *200*, 129 – 139.
- (4) Khan, W.; Betzler, S.; Šipr, O.; Ciston, J.; Blaha, P.; Scheu, C.; Minar, J. Theoretical and Experimental Study on the Optoelectronic Properties of $\text{Nb}_3\text{O}_7(\text{OH})$ and Nb_2O_5 Photoelectrodes. *J. Phys. Chem. C* **2016**, *120*, 23329–23338.

- (5) Yan, L.; Rui, X.; Chen, G.; Xu, W.; Zou, G.; Luo, H. Recent advances in nanostructured Nb-based oxides for electrochemical energy storage. *Nanoscale* **2016**, *8*, 8443–8465.
- (6) Brezesinski, K.; Wang, J.; Haetge, J.; Reitz, C.; Steinmueller, S.; Tolbert, S.; Smarsly, B.; Dunn, B.; Brezesinski, T. Pseudocapacitive Contributions to Charge Storage in Highly Ordered Mesoporous Group V Transition Metal Oxides with Iso-Oriented Layered Nanocrystalline Domains. *J. Am. Chem. Soc.* **2010**, *132*, 6982–6990, PMID: 20433176.
- (7) Augustyn, V.; Come, J.; Lowe, M.; Kim, J.; Taberna, P.-L.; Tolbert, S.; Abruña, H.; Simon, P.; Dunn, B. High-rate Electrochemical Energy Storage Through Li^+ Intercalation Pseudocapacitance. *Nature Mater.* **2013**, *12*, 1–5.
- (8) Chen, D.; Wang, J.-H.; Chou, T.-F.; Zhao, B.; El-Sayed, M.; Liu, M. Unraveling the Nature of Anomalously Fast Energy Storage in T-Nb₂O₅. *J. Am. Chem. Soc.* **2017**, *139*, 7071–7081, PMID: 28441872.
- (9) Cava, R.; Batlogg, B.; Krajewski, J.; Gammel, P.; Poulsen, H.; Peck, W. J.; Rupp, L. J. Antiferromagnetism and metallic conductivity in Nb₁₂O₂₉. *Nature* **1991**, *350*, 598–600.
- (10) Ohsawa, T.; Okubo, J.; Suzuki, T.; Kumigashira, H.; Oshima, M.; Hitosugi, T. An n-Type Transparent Conducting Oxide: Nb₁₂O₂₉. *J. Phys. Chem. C* **2011**, *115*, 16625–16629.
- (11) Le Viet, A.; Jose, R.; Reddy, M. V.; Chowdari, B. V. R.; Ramakrishna, S. Nb₂O₅ Photoelectrodes for Dye-Sensitized Solar Cells: Choice of the Polymorph. *J. Phys. Chem. C* **2010**, *114*, 21795–21800.
- (12) Ou, J.; Rani, R.; Ham, M.-H.; Field, M.; Zhang, Y.; Zheng, H.; Reece, P.; Zhuiykov, S.; Sriram, S.; Bhaskaran, M.; Kaner, R.; Kalantar-zadeh, K. Elevated Temperature Anodized Nb₂O₅: A Photoanode Material with Exceptionally Large Photoconversion Efficiencies. *ACS Nano* **2012**, *6*, 4045–4053, PMID: 22512314.

- (13) Gai, P.; Montero, J.; Lee, A.; Wilson, K.; Boyes, E. In situ Aberration Corrected-Transmission Electron Microscopy of Magnesium Oxide Nanocatalysts for Biodiesels. *Catal. Lett.* **2009**, *132*, 182–188.
- (14) Lee, G.-H.; Zuo, J.-M. TEM observation of growth and phase transformation in nanometer-sized titanium oxide powder. *J. Mater. Sci.* **2011**, *46*, 1780–1788.
- (15) Guo, H.; Khan, M.; Cheng, C.; Fan, W.; Dames, C.; Wu, J.; A.M., M. Vanadium dioxide nanowire-based microthermometer for quantitative evaluation of electron beam heating. *Nature Commun.* **2014**, *5*, 4986–4991.
- (16) Huang, C.-W.; Kuo, S.-S.; Hsin, C.-L. Electron-beam-induced phase transition in the transmission electron microscope: the case of VO₂(B). *CrystEngComm* **2018**, *20*, 6857–6860.
- (17) Naito, M.; Ishimaru, M.; Valdez, J. A.; Sickafus, K. E. Electron irradiation-induced phase transformation in α -FeSi₂. *Journal of Applied Physics* **2008**, *104*, 073524.
- (18) Sutter, E.; Huang, Y.; Komsa, H.-P.; Ghorbani-Asl, M.; Krasheninnikov, A.; Sutter, P. Electron-Beam Induced Transformations of Layered Tin Dichalcogenides. *Nano Lett.* **2016**, *16*, 4410–4416.
- (19) Padhi, S.; Gottapu, S.; Krishna, M. G. Electron-beam irradiation induced transformation of Cu₂(OH)₃NO₃ nanoflakes into nanocrystalline CuO. *Nanoscale* **2016**, *8*, 11194–11201.
- (20) Betzler, S.; Harzer, T.; Ciston, J.; Dahmen, U.; Dehm, G.; Scheu, C. Heat-Induced Phase Transformation of Three-Dimensional Nb₃O₇(OH) Superstructures: Effect of Atmosphere and Electron Beam. *Cryst. Growth & Des.* **2016**, *16*, 4309–4317.
- (21) Crozier, P.; Wang, R.; Sharma, R. In situ environmental TEM studies of dynamic

- changes in cerium-based oxides nanoparticles during redox processes. *Ultramicroscopy* **2008**, *108*, 1432 – 1440.
- (22) Koh, A. L.; Gidcumb, E.; Zhou, O.; Sinclair, R. Observations of Carbon Nanotube Oxidation in an Aberration-Corrected Environmental Transmission Electron Microscope. *ACS Nano* **2013**, *7*, 2566–2572, PMID: 23360330.
- (23) Koh, A. L.; Gidcumb, E.; Zhou, O.; Sinclair, R. Oxidation of Carbon Nanotubes in an Ionizing Environment. *Nano Letters* **2016**, *16*, 856–863, PMID: 26726919.
- (24) Narayan, T. C.; Hayee, F.; Baldi, A.; Koh, A.; Sinclair, R.; Dionne, J. Direct visualization of hydrogen absorption dynamics in individual palladium nanoparticles. *Nat. Commun.* **2017**, *8*, 14020.
- (25) He, M.; Wang, X.; Zhang, S.; Jiang, H.; Cavalca, F.; Cui, H.; Wagner, J. B.; Hansen, T. W.; Kauppinen, E.; Zhang, J.; Ding, F. Growth kinetics of single-walled carbon nanotubes with a $(2n, n)$ chirality selection. *Science Advances* **2019**, *5*.
- (26) Betzler, S.; Wisnet, A.; Breitbach, B.; Mitterbauer, C.; Weickert, J.; Schmidt-Mende, L.; Scheu, C. Template-free Synthesis of Novel, Highly-ordered 3D Hierarchical $\text{Nb}_3\text{O}_7(\text{OH})$ Superstructures with Semiconductive and Photoactive Properties. *J. Mater. Chem. A* **2014**, *2*, 12005–12013.
- (27) Betzler, S.; Podjaski, F.; Beetz, M.; Handloser, K.; Wisnet, A.; Handloser, M.; Hartschuh, A.; Lotsch, B.; Scheu, C. Titanium doping and its effect on the morphology of three-dimensional hierarchical $\text{Nb}_3\text{O}_7(\text{OH})$ nanostructures for enhanced light-induced water splitting. *Chem. Mater.* **2016**, *28*, 7666–7672.
- (28) Knotek, M.; Feibelman, P. Stability of ionically bonded surfaces in ionizing environments. *Surf. Sci.* **1979**, *90*, 78 – 90.
- (29) Jiang, N. Electron beam damage in oxides: a review. *Rep. Prog. Phys.* **2016**, *79*, 016501.

- (30) Egerton, R. Control of Radiation Damage in the TEM. *Ultramicroscopy* **2013**, *127*, 100 – 108, Frontiers of Electron Microscopy in Materials Science.
- (31) Betzler, S.; Koh, A.; Lotsch, B.; Scheu, C.; Sinclair, R. Preventing Electron Beam Induced Radiation Damage in a Niobium Oxide System Using a Gas Atmosphere. *submitted* **2020**, *xyz*, *xyz*.
- (32) Bach, D.; Schneider, R.; Gerthsen, D.; Verbeeck, J.; Sigle, W. EELS of Niobium and Stoichiometric Niobium-Oxide Phases—Part I: Plasmon and Near-Edges Fine Structure. *Microsc. Microanal.* **2009**, *15*, 505–523.
- (33) Groen, J. C.; Zhu, W.; Brouwer, S.; Huynink, S. J.; Kapteijn, F.; Moulijn, J. A.; Pérez-Ramírez, J. Direct Demonstration of Enhanced Diffusion in Mesoporous ZSM-5 Zeolite Obtained via Controlled Desilication. *Journal of the American Chemical Society* **2007**, *129*, 355–360, PMID: 17212415.
- (34) Zheng, H.; Zhai, D.; Zhao, L.; Zhang, C.; Yu, S.; Gao, J.; Xu, C. Insight into the contribution of isolated mesopore on diffusion in hierarchical zeolites: The effect of temperature. *Industrial & Engineering Chemistry Research* **2018**, *57*, 5453–5463.
- (35) Schäfer, H.; Gruehn, R.; Schulte, F. The Modifications of Niobium Pentoxide. *Angew. Chem. Int. Ed.* **1966**, *5*, 40–52.
- (36) Rani, R.; Zoolfakar, A.; O’Mullane, A.; Austin, M.; Kalantar-Zadeh, K. Thin films and nanostructures of niobium pentoxide: fundamental properties, synthesis methods and applications. *J. Mater. Chem. A* **2014**, *2*, 15683–15703.
- (37) Li, S.; Xu, Q.; Uchaker, E.; Cao, X.; Cao, G. Comparison of amorphous, pseudo-hexagonal and orthorhombic Nb₂O₅ for high-rate lithium ion insertion. *CrystEngComm* **2016**, *18*, 2532–2540.

- (38) Kato, K.; Tamura, S. Die Kristallstruktur von T-Nb₂O₅. *Acta Cryst. B* **1975**, *31*, 673–677.
- (39) Weissman, J. G.; Ko, E. I.; Wynblatt, P.; Howe, J. M. High-resolution electron microscopy and image simulation of TT-,T-, and H-niobia and model silica-supported niobium surface oxides. *Chem. Mater.* **1989**, *1*, 187–193.
- (40) Griffith, K.; Forse, A.; Griffin, J.; Grey, C. High-Rate Intercalation without Nanostructuring in Metastable Nb₂O₅ Bronze Phases. *J. Am. Chem. Soc.* **2016**, *138*, 8888–8899, PMID: 27264849.
- (41) Martin, M. *Diffusion in Oxides*; 2005; pp 209–247.
- (42) Shirane, G.; Danner, H.; Pepinsky, R. Neutron Diffraction Study of Orthorhombic BaTiO₃. *Phys. Rev.* **1957**, *105*, 856–860.
- (43) Rollinson, H.; Adetunji, J. In *Encyclopedia of Geochemistry: A Comprehensive Reference Source on the Chemistry of the Earth*; White, W., Ed.; Springer International Publishing: Cham, 2018; pp 738–743.
- (44) Hu, S. M. Formation of stacking faults and enhanced diffusion in the oxidation of silicon. *J. Appl. Phys.* **1974**, *45*, 1567–1573.
- (45) Balluffi, R. W.; Olson, G. B. On the Hierarchy of Interfacial Dislocation Structure. *Metall. Trans. A* **1985**, *16*, 529–541.
- (46) Zheng, H.; Rivest, J.; Miller, T.; Sadtler, B.; Lindenberg, A.; Toney, M.; Wang, L.-W.; Kisielowski, C.; Alivisatos, A. Observation of Transient Structural-Transformation Dynamics in a Cu₂S Nanorod. *Science* **2011**, *333*, 206–209.
- (47) Liu, H.; Zheng, L., H. and Li; Sheng, H.; Jia, S.; Cao, F.; Liu, X.; Chen, B.; Xing, R.; Zhao, D.; Wang, J. Atomic-scale observation of a two-stage oxidation process in Cu₂O. *Nano Res.* **2017**, *10*, 2344–2350.

4 Graphical TOC Entry

